ACS APPLIED MATERIALS & INTERFACES

Research Article

www.acsami.org

Versatile Particle-Based Route to Engineer Vertically Aligned Silicon Nanowire Arrays and Nanoscale Pores

Roey Elnathan,[#,†] Lucio Isa,[#,‡] Daniel Brodoceanu,[§] Adrienne Nelson,[‡] Frances J. Harding,[†] Bahman Delalat,[†] Tobias Kraus,[§] and Nicolas H. Voelcker*[,†]

[†]ARC Centre of Excellence in Convergent Bio-Nano Science and Technology, Future Industries Institute, University of South Australia, Adelaide, SA 5001, Australia

[‡]Laboratory for Interfaces, Soft Matter and Assembly, Department of Materials, ETH Zurich, Vladimir-Prelog-Weg 5, 8093 Zurich, Switzerland

[§]INM—Leibniz Institute for New Materials, Campus D2 2, Saarbrücken 66123, Germany

Supporting Information

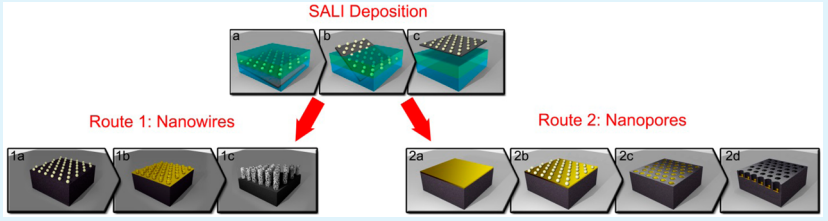

ABSTRACT: Control over particle self-assembly is a prerequisite for the colloidal templating of lithographical etching masks to define nanostructures. This work integrates and combines for the first time bottom-up and top-down approaches, namely, particle self-assembly at liquid—liquid interfaces and metal-assisted chemical etching, to generate vertically aligned silicon nanowire (VA-SiNW) arrays and, alternatively, arrays of nanoscale pores in a silicon wafer. Of particular importance, and in contrast to current techniques, including conventional colloidal lithography, this approach provides excellent control over the nanowire or pore etching site locations and decouples nanowire or pore diameter and spacing. The spacing between pores or nanowires is tuned by adjusting the specific area of the particles at the liquid—liquid interface before deposition. Hence, the process enables fast and low-cost fabrication of ordered nanostructures in silicon and can be easily scaled up. We demonstrate that the fabricated VA-SiNW arrays can be used as in vitro transfection platforms for transfecting human primary cells.

KEYWORDS: *nanomaterials, vertically aligned silicon nanowires, colloidal lithography, human cells, nanobio interfaces, gene delivery*

1. INTRODUCTION

Over the past decade, progress in lithography and fabrication tools has enabled the production of nanomaterials with well-defined architectures.[1,2] Among the range of explored nanomaterial structures, vertically aligned silicon nanowire (VA-SiNW) arrays constitute a prime example, where the presence of controlled nanoscale topography holds the key to a large range of diverse applications, from multispectral imaging[3] to the development of nano-biocellular interfaces.[4] In all cases, control of the geometrical parameters of the nanowires (NWs) holds the key to their successful application and integration in devices.[5−7] For the specific case of cell—nanotopography interactions, VA-SiNW arrays have proven to play a central role in controlling cellular function and behavior based on the geometry of the NWs.[8] Particularly, engineered VA-SiNW arrays have shown their potential to serve as an effective transfection platform for gene delivery through mechanical transfection via the NWs[8,10,9]. Very recently, significant developments have occurred in regards to the integration of porous and degradable VA-SiNW arrays fabricated by metal-assisted chemical etching (MACE), for instance, demonstrating sustained neovascularization in muscle tissue via intradermal delivery[10] and live intracellular sensing of pH.[11] Taken together, these pioneering studies have significantly advanced the use of VA-SiNWs to create smart and functional NW—cell interfaces. This research has generated a strong demand for efficient and cost-effective routes to fabricate VA-SiNW arrays.

In parallel, arrays of nanoscale pores on Si are attractive for a variety of applications, including solar cells,[12,13] Li-ion batteries,[14] biosensors,[15] templates for polymer replica molding,[16] enzyme nanoreactors[1] for the detection of small molecules via surface-assisted laser desorption/ionization, mass spectrometry,[17] and for the fabrication of antireflective surfaces. Similarly to the case of the VA-SiNWs, the geometrical parameters of the pore arrays, that is, their diameter and spacing, are also crucial to determine their functionality and performance.[1]

Received: August 20, 2015
Accepted: October 2, 2015
Published: October 2, 2015

DOI: 10.1021/acsami.5b07777
ACS Appl. Mater. Interfaces 2015, 7, 23717−23724

Arrays of VA-NWs or pore arrays can be generated by several fabrication methods, including bottom-up epitaxy-based vapor−liquid−solid (VLS) growth,[18] metal−organic vapor-phase epitaxy (MOVPE),[19] and top-down approaches such as reactive-ion etching (RIE),[20] ion- or e-beam lithography,[20] and MACE.[21] Each of these fabrication processes has drawbacks and limitations: VLS growth requires specific Si substrates, employs expensive setups to handle hazardous silane gases at high temperatures, and is generally restricted to circular-shaped gold catalysts.[22] Additionally, the limited ability to control positioning, orientation, and density of VLS-generated NWs in arrays renders studies of NW−cell interactions of little use.[8] RIE only achieves a limited NW aspect ratio, and, most importantly, the high cost and poor accessibility of these fabrication processes restrict their use to a few laboratories. Sequential fabrication by means of ion or e-beam lithography affords high accuracy, but at the expense of speed, scale, and cost-effectiveness.

Combining conventional colloidal/nanosphere lithography (NSL) and MACE, large areas of arrays can be produced cheaply and in parallel, but sacrificing flexibility and control over the geometrical parameters of the pattern. In fact, in NSL-based patterning, monolayers of nanoparticles are used to produce lithography masks. There are several ways to deposit the particles, either directly from solution,[23] via spin-coating,[24] controlled evaporation,[25] or by means of convective assembly[26,27] and electrophoretic deposition.[28,29] The main limitation of NSL is that, using the conventional approaches described above, typically close-packed arrays of particles are formed on the substrates or in arrays where the interparticle separation is significantly smaller than the particle size. Alternatives exist, where the interparticle distance can be increased by etching the deposited colloids, for example, in an oxygen plasma.[30,31] Nevertheless, feature size and separation are not independently controlled but are linked by the initial particle size. Furthermore, there are limitations in the shrinking ratio, before the morphology of the etched particles start to deviate uncontrollably from the spherical shape.

In this work, we show that these limitations can be overcome by using self-assembly at liquid−liquid interfaces (SALI) deposition. This strategy enables the production of tunable nonclose packed (ncp) particle arrays, exploiting nanoparticle trapping at a fluid interface, combined with the harnessing of long-ranged electrostatic repulsion between nanoparticles within the interface plane.[32] Here, separation and feature size are independently tuned, where the former is controlled by adjusting the specific area per particle at the interface and the latter is fixed by the particle size. After deposition, the nanoparticle arrays are used as masks for MACE. Our alternative strategy enables the fabrication of nanopatterns in silicon combining the flexibility of SALI with the etching selectivity and simplicity of MACE. We demonstrate the use of this process to produce arrays of VA-SiNW and, alternatively, arrays of nanoscale pores in a silicon wafer. This combined approach allows facile control over the etching sites, where, critically, the spacing and the diameter of the SiNW or pore elements are independently controlled. We furthermore demonstrate that the VA-SiNW arrays are an effective platform for gene delivery to primary human cells.

2. EXPERIMENTAL SECTION

Preparation of Si Wafers. Prior to the amidine polystyrene latex (A-PS, Life Techologies, USA) deposition, flat silicon wafers (p-type, 3−6 Ω cm and 10−20 mΩ cm, ⟨100⟩) were cut into roughly 1 × 1 cm^2 pieces, cleaned by sonication in acetone and isopropanol, washed with deionized water (Millipore), and then blow-dried with a nitrogen jet stream. This was followed by UV−ozone cleaning for 2 min to remove organic contaminants and to render the silicon substrates hydrophilic.

Liquid−Liquid Interface Deposition. A 50 mL polypropylene centrifuge tube was filled with 40 mL of Milli-Q water. The wafer was lowered into the water on a holder with an angle of 30°, and 7 mL of hexane (≥95%) was added carefully on top. A needle connected to a peristaltic pump containing 0.02−0.08% solution of A-PS (0.5, 0.2, 0.1 μm diameter) in a 60:40 mixture of Milli-Q water/2-propanol was inserted into the centrifuge tube, and the tip of the needle was positioned at the interface between the hexane and water. The solution was then injected at a speed of 0.5 μL/s to a specified volume, and the needle was withdrawn. The A-PS at the interface rearranged into open crystals, due to the long-range electrostatic repulsions between them. Next, the wafer was extracted at 25 μm/s through the water−hexane interface and subsequently the hexane−air interface. To ensure transfer of the interfacial crystalline pattern, the speed of extraction was controlled to be equal to (or lower than) the rate of hexane evaporation to prevent a drying meniscus forming across the sample, which can lead to particle rearrangement.

Preparation of VA-SiNW Arrays. Samples prepared by SALI deposition were inserted into a standard direct current (DC) magnetron sputtering system (JEOL, JFC-1300, Japan). The sputtering was performed for 80 s using an argon pressure of 0.08 mbar and a 30 mA discharge current to deposit gold films with thicknesses of 30−50 nm. All etching solutions were prepared with HF concentrations of 4.8 and 0.1 M H_2O_2 in Milli-Q water. Reactions were conducted in a standard Teflon container at room temperature for different times to achieve the desired SiNW length. The A-PS were then removed by sonication in Milli-Q water for 20 s.

Preparation of the Submicron Pore Arrays. Gold layers with thicknesses of 30−50 nm were sputtered (JEOL, JFC-1300, Japan) for 80 s at 0.08 mbar of argon pressure and 30 mA of discharge current. Deposition (SALI): the same procedure as above was used, employing only the 0.5 μm diameter A-PS particles. The gold-coated silicon samples with the ncp A-PS monolayer assembled on top was fixed on a 2-in. copper disc holder using carbon tape. The copper holder was then mounted on the DC sputter head (cathode), acting as a target for the argon ions. The chamber was pumped to about 0.1 mbar and flushed with argon to remove adsorbed gas contaminants. When the argon gas reached the operation pressure (0.08 mbar), the sputtering process started at a discharge current of 20 mA and continued for a duration of 20 s. The A-PS particles were peeled off using an adhesive tape. The etching solutions were prepared with HF concentrations of 4.8 and 0.1 M H_2O_2. The reactions were conducted at room temperature for 12 min. During the etching process the reaction vessels were knocked at regular intervals to remove the hydrogen bubbles generated on the silicon sample during the MACE process, as they may negatively impact the orientation of the etched pores. After etching, the samples were thoroughly washed with deionized water and dried with nitrogen.

Cell Culture. Human dental pulp mesenchymal stem cells (hDPSC) were grown and maintained at 37 °C with 5% CO_2 in Dulbecco's modified eagle medium (DMEM) supplemented with 10% fetal bovine serum (FBS), 2 mM L-glutamine, 100 U/mL penicillin, and 100 μg/mL streptomycin, for 2−3 d until they were 70−80% confluent. After trypsinization, cells were seeded at a density of 5 × 10^4 cells/mL in complete DMEM onto the substrates.

Cell Transfection. Cells were cultured in DMEM medium supplemented with 10% FBS, 2 mM L-glutamine, 100 U/mL penicillin, and 100 μg/mL streptomycin, then incubated at 37 °C in a fully humidified atmosphere with 5% CO_2, and the medium was exchanged twice a week. The adherent cells were detached and harvested by using a 0.05% trypsin/ethylenediaminetetraacetic acid solution treatment. Serial passaging (1:3 split) at 70−80% confluency was performed. To transfect gWIZ GFP plasmid into hDPSC cells, we placed the VA-NW substrates in a 24-well sterile format. The substrates were then

DOI: 10.1021/acsami.5b07777
ACS Appl. Mater. Interfaces 2015, 7, 23717−23724

Scheme 1. Schematic Describing the Fabrication Process[a]

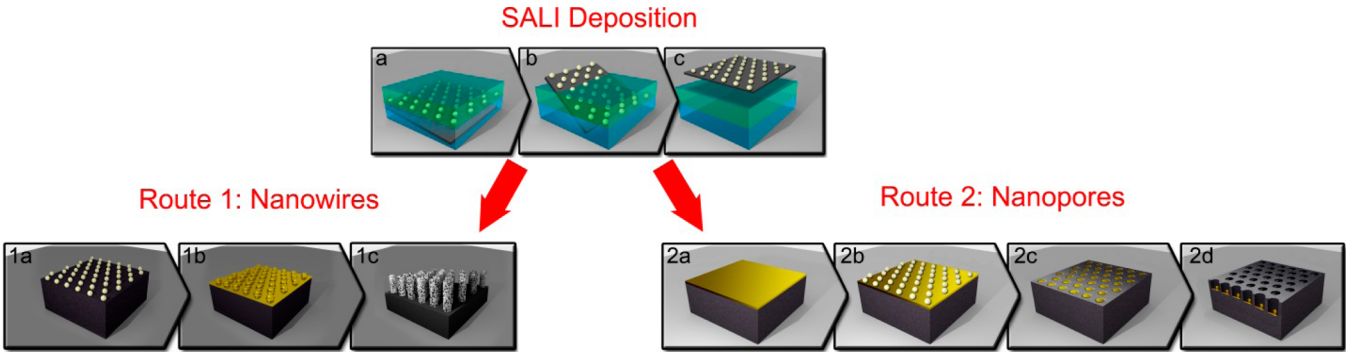

[a]The top row indicates the steps for the SALI deposition of tunable colloidal lithography masks using SALI. The route 1 and route 2 bottom rows describe the two different fabrication routes to obtain arrays of SiNWs or nanoscale pores, respectively. (upper) (a) Self-assembly of amidine latex polystyrene particles at the water/*n*-hexane interface. Electrostatic repulsion between the particles at the interface generates ncp particle arrays. (b, c) The particles are deposited onto a solid substrate through lift-off at controlled velocity. Route 1 NW fabrication: (1a,b) The nanoparticle array is coated by a thin gold layer and the particles provide masking for MACE. (1c) MACE produces arrays of VA-SiNWs (after removal of the gold layer). The process selectively etches the underlying silicon wafer around the deposited particles, leading to the formation of NW arrays. Route 2 Nanopore fabrication: (2a) Silicon wafers are coated with an Au-layer. (2b) The colloidal particles are deposited from the water/*n*-hexane interface onto the Au-coated silicon wafer. (2c) Metal disk arrays are produced after sputter-etching and subsequent lift-off of particles. In this case, the colloids act as masks for the sputter-etching. (2d) Ncp arrays of submicron pores etched into silicon via MACE of the gold disks.

sterilized in 70% ethanol and were allowed to dry at room temperature for 2 h in a laminar flow cabinet. Following this, the substrates were coated with poly-D-lysine at concentration of 167 μg/L and incubated at 4 °C for 4 h, followed by washing step with phosphate-buffered saline (PBS). gWIZ GFP plasmid was diluted to 20 μg/mL in PBS, and 100 μL of this solution was added per well on top of the substrate. The substrates were then incubated at 4 °C overnight, and unbound plasmid was washed with PBS. Cells were seeded at density of 5×10^4 cells/mL in Opti-MEM onto the substrates. The samples were then incubated for 4−6 h at 37 °C in a humidified atmosphere with 5% CO_2. Subsequently, the Opti-MEM medium was replaced with regular medium containing DMEM, FBS 10% and incubated at 37 °C for 48−72 h.

The cells for Lipofectamine transfection were seeded at a density of 5×10^4 cells/mL in complete DMEM onto the sterile flat silicon wafers in a 24-well sterile format at 37 °C and 5% CO_2. After 1 d of incubation, 20 μL of Lipofectamine 2000 and 20 μg of gWIZ GFP plasmid were both diluted in separate microfuge tubes filled with 500 μL of Opti-MEM. After 5 min the solutions were combined and mixed by pipetting up and down once. The mixture was incubated at room temperature for 20 min, dropwise added to the cells, and mixed by swirling the plate. After 6 h of incubation at 37 °C and 5% CO_2, medium was replaced with fresh complete medium containing DMEM, FBS 10% and incubated at 37 °C for 72 h.

Determination of Transfection Efficiency. To assess the efficiency of delivery of eGFP reporter gene, the fraction of cells exhibiting green fluorescence was determined after 60 h of incubation. SiNW diameter: 400 nm, average heights and spacing of 1.2 and 1.3 μm, respectively. hDPSCs counted: 22, transfection efficiency: 77%.

Scanning Electron Microscopy Imaging. SEM imaging was performed using three types of instruments, namely, a Zeiss LEO 1350, a Quanta 450 FEG Environmental SEM (FEI, Netherlands), and a FEI Quanta 400F scanning electron microscope (FEI Europe, Eindhoven).

Optical Imaging. Optical images of the deposited A-PS particle arrays where acquired in reflection mode at 50× and 100× magnification with an upright Zeiss Axioscope 2 optical microscope.

Confocal Imaging. The cell samples were washed with PBS and then fixed in a solution of 4% paraformaldehyde in PBS (pH = 7.4) for 10 min, followed by permeabilization in PBS-0.25% Triton X-100 for 5 min at room temperature. After they were washed at room temperature in PBS three times for 5 min each, cell nuclei were stained with Hoechst 33342 at a final concentration of 2 μg/mL for 10 min at room temperature. Confocal imaging was performed using a Nikon A1R confocal laser scanning microscope system in V1−07A. GFP and Hoechst 33342 fluorescence were excited using the 488 nm argon laser line and the 405 nm laser, respectively. The fixed hDPSC were analyzed determined using the Nikon NIS-Elements software provided by the manufacturer.

Image Processing and Analysis. Fluorescence microscopy images were statistically analyzed by Wimasis Image Analysis. Optical and SEM images were processed and analyzed with ImageJ and with custom particle location software written in Interactive Data Language (IDL, ITT Visual Information Solutions). The contrast and the brightness were not varied from the original images.

3. RESULTS AND DISCUSSION

A combination of SALI and MACE was used to fabricate ordered VA-SiNW and nanoscale pore arrays. This process involves several distinct steps, summarized in Scheme 1. A distinct feature of the process is that the mask is produced in the same way to obtain both final nanostructures, and only the subsequent etching steps differ. Fabrication began with the formation of ncp colloidal arrays at a water/*n*-hexane interface exploiting SALI. Controlled volumes of the particle suspensions were injected directly at the interface using a water/isopropanol spreading solution and a microsyringe connected to a peristaltic pump. Electrostatic repulsive interactions (dipole−dipole) at the interface are responsible for the formation of ncp arrays,[33] while the particles stay confined within the interface plane due to strong vertical trapping[34] (Scheme 1 upper (a)). The patterns were then successfully transferred onto a solid substrate by lifting the latter through the interface using a linear motion drive[32] (Scheme 1 upper b,c). SALI has been used for deposition of particles with sizes ranging from 40 nm to several microns, but the use of large colloids requires more complex and delicate drying procedures to prevent particle aggregation[35] compared to the simple lift-off presented here. The deposition was performed either on bare low-resistivity silicon wafers or on wafers coated by a thin layer of gold. In the first case, the nanoparticle arrays were used as masks for the fabrication of Si-NW arrays (Route 1); in the other case, arrays of nanoscale pores were fabricated (Route 2). More details on

DOI: 10.1021/acsami.5b07777
ACS Appl. Mater. Interfaces 2015, 7, 23717−23724

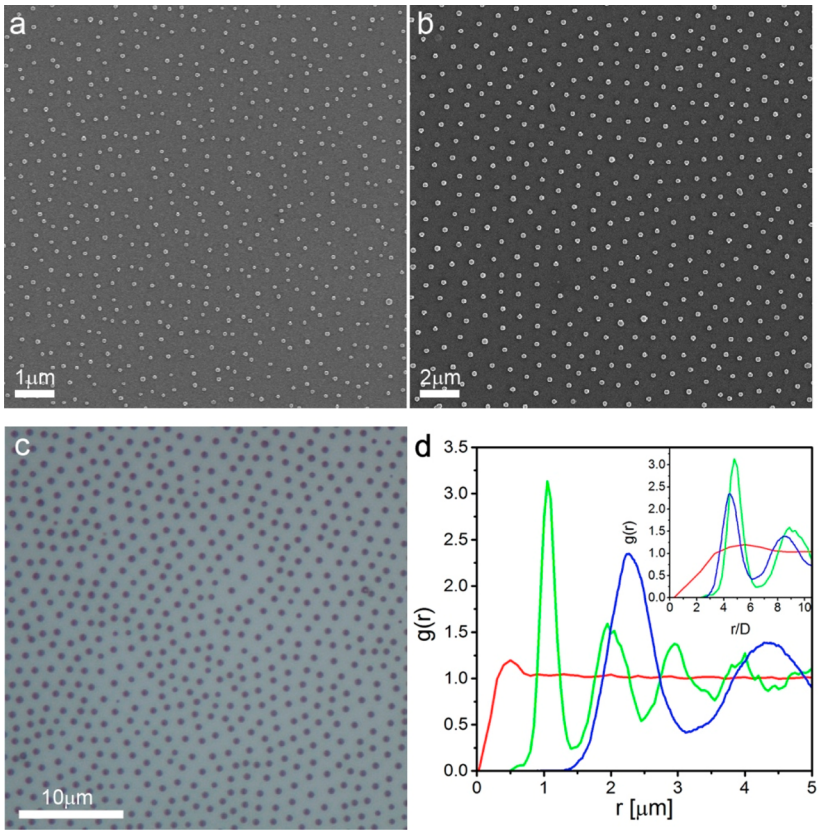

Figure 1. SALI particle deposition. Micrographs of SALI particle depositions of (a-SEM) 100, (b-SEM) 200, and (c-Optical) 500 nm diameter amidine latex nanoparticles (A-PS) deposited on Si at the same surface coverage. (d) Corresponding particle radial distribution functions $g(r)$. Red curve: 100 nm diameter A-PS, green: 200 nm, blue: 500 nm. The position of the first peak indicates the average interparticle spacing. For the 100 nm diameter particles only the nearest neighbors ordering is visible. (inset) $g(r)$ vs distance normalized by particle diameter, highlighting that in all images there is an ∼5 particle diameter separation between the particles.

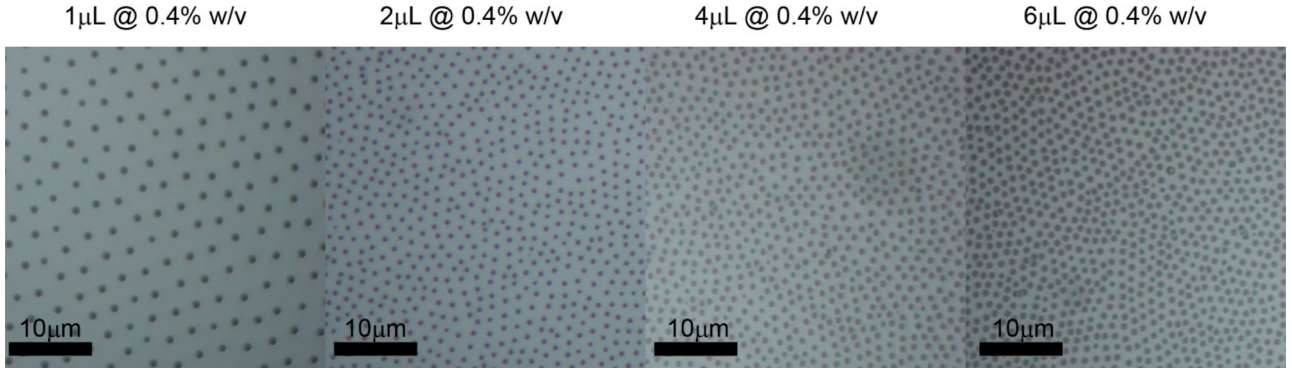

Figure 2. Optical images of 500 nm amidine polystyrene latex particles of increasing surface coverage (controlled by injection volume) deposited onto a 1 × 1 cm^2 Si wafer after SALI at the water/*n*-hexane interface.

the experimental procedures are found in the Supporting Information and in the Experimental Section.

In this work, we used SALI to deposit amidine polystyrene latex (A-PS) particles of three different diameters 100, 200, and 500 nm at a controlled area density at the interface, tuned by the injected volume. Figure 1a–c shows the resulting patterns for particles of these three diameters at the same surface coverage on a silicon wafer. For 500 and 200 nm diameter particles, the deposition led to the formation of polycrystalline monolayers with local hexagonal ordering, as visible in the radial distribution functions of Figure 1d. In the case of the 100 nm diameter particles, at this surface coverage, the electrostatic interactions were too weak to induce local crystallization; however, a defined nearest neighbor distance was still present, and electrostatic repulsion prevented aggregation of the particles at the interface. Hence, the surface coverage of the features was still well-defined and controlled over large areas, even in the absence of long-range order. In addition, the interparticle spacing in the arrays could be adjusted by tuning the number of particles injected at the interface.

Figure 2 shows a series of optical images of 500 nm diameter particles of increasing surface coverage. The diameter of the deposited particles determines the diameter of the nanowires/pores, and their separation is controllable by simply adjusting

DOI: 10.1021/acsami.5b07777
ACS Appl. Mater. Interfaces 2015, 7, 23717–23724

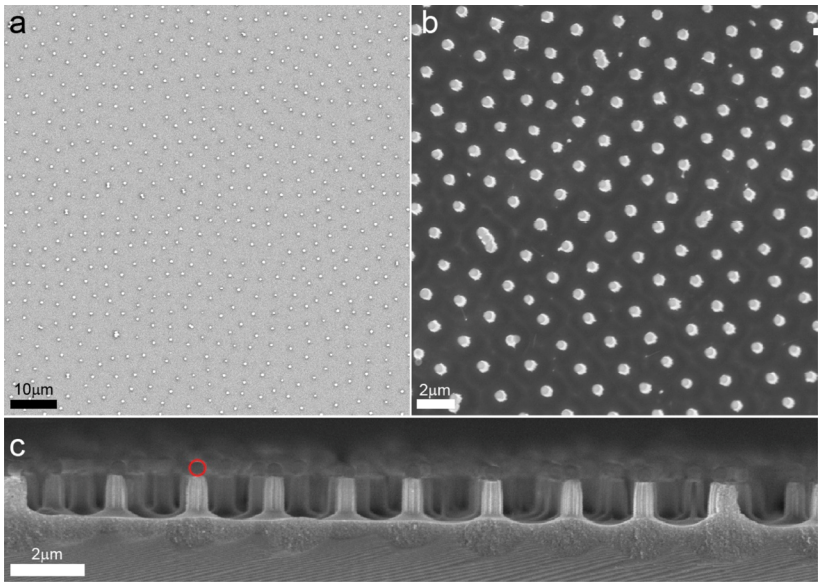

Figure 3. Fabrication of VA-SiNW arrays using SALI and MACE. (a) 500 nm amidine latex polystyrene particles were assembled on a Si wafer creating an ncp monolayer (SEM image). The array was used as a mask for the deposition of a Au layer by sputter-coating. (b) Representative SEM image showing a top view of VA-SiNW arrays obtained by MACE. (c) The corresponding cross-section SEM image. The red circle outlines an example of colloidal particles that are still visible on top of the NWs. Average NW dimensions: center-to-center separation = 2.1 ± 0.2 μm, diameter = 510 ± 20 nm, and length = 1.16 ± 0.2 μm.

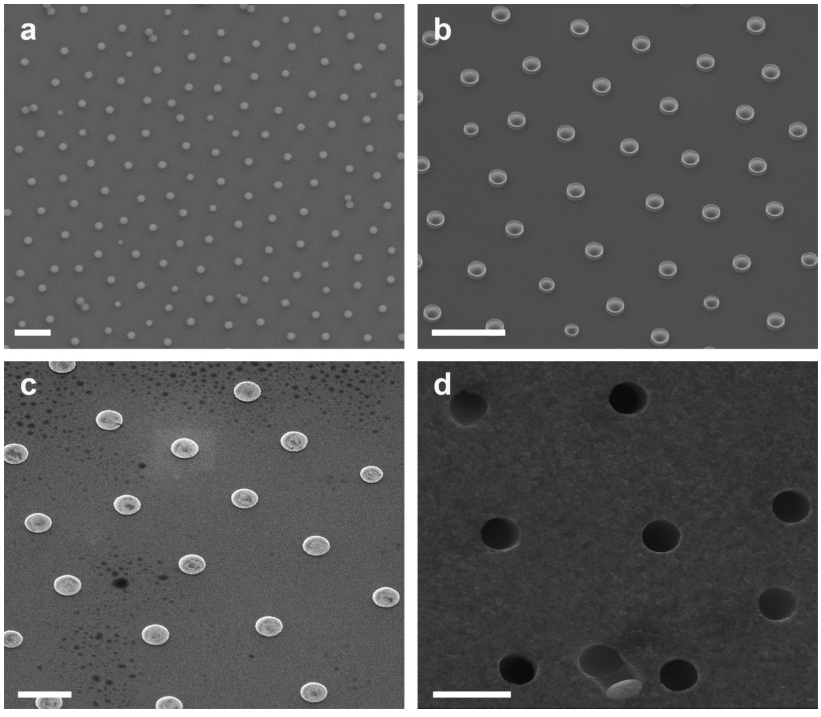

Figure 4. Nanoscale pore array fabrication process. (a) Patterns (ncp) of A-PS particles (500 nm) assembled on a gold-coated silicon wafer. (b) SEM image of metal disc array after sputter etching process and (c) subsequent removal of the remaining PS particles. (d) Array of pores etched (1.8 μm average depth) into silicon via MACE using Au disk array as catalysts. Scale bars represent 2 μm (a, b) and 1 μm (c, d).

the volume of injected particles into a sample cell with fixed cross section. Figure S1 shows that the interparticle separation correlates with the injected suspension volume.

The deposited particle monolayer (Scheme 1a) was then used as a direct mask for the deposition of a gold layer by sputter-coating on top of the particle arrays, Scheme 1b, Figure 3a. The Au layer was used as a catalyst material for the fabrication of ordered arrays of VA-SiNW with controlled diameter, length, and spacing via MACE, Scheme 1c. Figure 3b,c shows top and cross-section view SEM images of SiNW arrays with the following average NW dimensions: diameter 510 nm, length 1.1 μm, spacing 2.1 μm. Finally, the particles residing on top of the array were lifted off by means of a short sonication step, Figure S2. The process yielded VA-SiNW arrays that replicated the lateral geometry of the particle mask. Note that the MACE process introduces porosity in the

DOI: 10.1021/acsami.5b07777
ACS Appl. Mater. Interfaces 2015, 7, 23717−23724

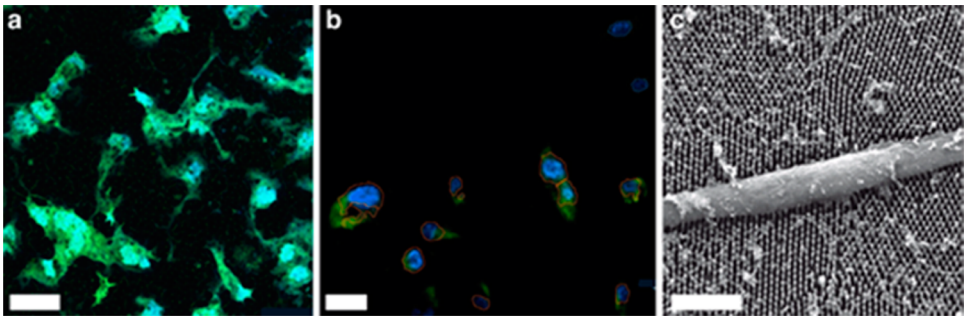

Figure 5. Interaction between primary hDPSC and VA-SiNW arrays. (a) Laser-scanning confocal microscopy image and (b) fluorescence microscopy image of eGFP transfected hDPSC (green color) cultured on VA-SiNW arrays, with NW spacing of 1.3 μm, average NW diameter of 400 nm, and average NW height of 1.2 μm. All cells were costained with nuclear dye Hoechst 33342 (blue). (c) SEM image of hDPSC adhering to an array of SiNW showing close cell−SiNW contact. Scale bar represent 25 μm (a), 50 μm (b), and 10 μm (c).

crystalline silicon within the nanowires and underneath them, as can be seen in Figure 3c.

Using the approach presented here, the SiNW diameter is solely dictated by the initial particle size. The SiNW length is independently controlled by the etching time, and the spacing in the array is determined by the electrostatic interactions between the particles and the number (volume) of the particles inserted at the water/*n*-hexane interface. All of these parameters are independent from each other and enable a fully flexible nanofabrication route.

The versatility of our combined fabrication strategy is effectively demonstrated by extending it to the production of nanoscale pore arrays, Figure 4. In contrast to other studies that reported the fabrication of pore arrays via convective assembly[1] and spin-coating techniques,[36] which require additional processing steps, the deposition of the nanoparticle patterns onto gold-coated silicon wafers offers a simpler and more effective route (Scheme 1, Route 2). Figure 4a shows a monolayer of 500 nm diameter particles on a wafer coated with 30 nm of Au; this is followed by sputter-etching of the gold using the particles as a direct mask, and the subsequent removal of the remaining particles for the formation of Au disk arrays (Figure 4b,c). The sputter-etching process induces etching of the gold around the particles. Finally, the Au disk arrays were used as catalysts in MACE process to produce pore arrays where the individual pore elements are straight and perpendicular to the silicon wafer. The average pore diameter is 500 nm, and average pore depth is 1.8 μm. In our previous work, we demonstrated the feasibility of fine-tuning the geometrical parameters of the dense pore arrays prepared using a combination of conventional NSL and MACE.[1] Here, we show that using SALI deposition sparser arrays can be produced, which, for instance, can find use in biosensing platforms to avoid cross-talk between different sensing hotspots.[37]

We finally demonstrate an application of the VA-SiNW arrays produced by our combined approach in cell transfection studies. We tested the feasibility of our VA-SiNW arrays as an in vitro platform for transfecting primary human dental pulp stem cells (hDPSC). This primary cell type is known to be responsive to nanotopographical cues and is hard to transfect by conventional methods.[38,39]

The fluorescence microscopy images in Figure 5a,b show transfected hDPSC cells with an average transfection efficacy of 77%. The SiNW arrays were first coated with poly-D-lysine (PDL). gWizTM high-expression enhanced green fluorescent protein vector (gWizTM eGFP) was employed as a reporter gene for successful plasmid DNA transfection. In Figure 5c, the array of VA-SiNWs (NW average dimensions of 400 nm diameter, 1.2 μm height, and 1.3 μm spacing) is shown that was used for this investigation.

This result was achieved with a VA-SiNW array without optimization of the NW array geometry (density, height, and diameter). For comparison, we transfected hDPSC with the cationic liposome Lipofectamine 2000 using the same plasmid and achieved 76% transfection efficiency. This preliminary result confirms the feasibility of using VA-SiNWs arrays to mediate cell transfection. A systematic study is currently in progress to assess how the SALI-produced VA-SiNW array geometry influences cell transfection.

4. CONCLUSION

Our results demonstrate assembly of polystyrene nanospheres into an ncp monolayer, producing a lithographical etching mask to grow NW and pore arrays of controlled diameter and spacing through MACE. Critically this technique decouples the parameters of NW and pore-element spacing and diameter, extending the combinatorial space of NW and pore geometry that can be fabricated. Arrays of VA-SiNW were prepared using the ncp arrays as masks during gold deposition on silicon followed by MACE. In contrast, arrays of Au disks were prepared, after SALI deposition on a Au-coated silicon wafer followed by sputter etching and removal of the A-PS particles. The Au disks then served as catalysts in MACE, generating nanoscale pores perpendicular to the silicon wafer. The results of our fabrication strategy will enable the screening of a large range of topographical parameters in studies using Si-NWs as platforms for cell transfection, a direction yet to be explored.

■ ASSOCIATED CONTENT

Supporting Information

The Supporting Information is available free of charge on the ACS Publications website at DOI: 10.1021/acsami.5b07777.

Chemicals and materials, plot of radial distribution function, plot of interparticle separation, SEM of VA-SiNW arrays. (PDF)

■ AUTHOR INFORMATION

Corresponding Author

*E-mail: nico.voelcker@unisa.edu.au.

DOI: 10.1021/acsami.5b07777
ACS Appl. Mater. Interfaces 2015, 7, 23717−23724

Author Contributions

[#]R.E. and L.I. contributed equally to this work. The manuscript was written through contributions of all authors. All authors have given approval to the final version of the manuscript.

Notes

The authors declare no competing financial interest.

■ ACKNOWLEDGMENTS

N.H.V. thanks the Alexander von Humboldt Foundation for a Fellowship for Experienced Researchers. D.B. and T.K. thank E. Arzt for his continuing support of the project. Funding from the German Science Foundation (DFG) in the framework of Priority Programme 1420, from the Australia−Germany Researcher Mobility Programme, the DAAD-ATN travel grant scheme, and the Australian Research Council Centre of Excellence in Convergent Bio-Nano Science and Technology (Project No. CE140100036) are gratefully acknowledged. L.I. acknowledges financial support from the Swiss National Science Foundation Grant No. PP00P2_144646/1.

■ ABBREVIATIONS

VA-SiNW, vertically aligned silicon nanowire
SALI, self-assembly at liquid−liquid interfaces
MACE, metal-assisted wet chemical etching
VLS, vapor−liquid−solid
CVD, chemical vapor deposition
MOVPE, metal organic vapor phase epitaxy
RIE, reactive-ion etching
NSL, nanosphere lithography
ncp, nonclose-packed
hcp, hexagonal close-packed
A-PS, amidine polystyrene latex
pDNA, plasmid DNA
hDPSC, human dental pulp stem cells

■ REFERENCES

(1) Brodoceanu, D.; Elnathan, R.; Prieto-Simón, B.; Delalat, B.; Guinan, T.; Kroner, E.; Voelcker, N. H.; Kraus, T. Dense Arrays of Uniform Submicron Pores in Silicon and Their Applications. *ACS Appl. Mater. Interfaces* **2015**, *7*, 1160−1169.

(2) Alhmoud, H.; Delalat, B.; Elnathan, R.; Cifuentes-Rius, A.; Chaix, A.; Rogers, M.-L.; Durand, J.-O.; Voelcker, N. H. Porous Silicon Nanodiscs for Targeted Drug Delivery. *Adv. Funct. Mater.* **2015**, *25*, 1137−1145.

(3) Park, H.; Crozier, K. B. Multispectral Imaging with Vertical Silicon Nanowires. *Sci. Rep.* **2013**, *3*, 2460.

(4) Elnathan, R.; Kwiat, M.; Patolsky, F.; Voelcker, N. H. Engineering Vertically Aligned Semiconductor Nanowire Arrays for Applications in the Life Sciences. *Nano Today* **2014**, *9*, 172−196.

(5) Alhmoud, H. Z.; Guinan, T. M.; Elnathan, R.; Kobus, H.; Voelcker, N. H. Surface-Assisted Laser Desorption/Ionization Mass Spectrometry using Ordered Silicon Nanopillar Arrays. *Analyst* **2014**, *139*, 5999−6009.

(6) Seo, K.; Wober, M.; Steinvurzel, P.; Schonbrun, E.; Dan, Y.; Ellenbogen, T.; Crozier, K. B. Multicolored Vertical Silicon Nanowires. *Nano Lett.* **2011**, *11*, 1851−1856.

(7) Krivitsky, V.; Hsiung, L. C.; Lichtenstein, A.; Brudnik, B.; Kantaev, R.; Elnathan, R.; Pevzner, A.; Khatchtourints, A.; Patolsky, F. Si Nanowires Forest-Based On-Chip Biomolecular Filtering, Separation and Preconcentration Devices: Nanowires Do it All. *Nano Lett.* **2012**, *12*, 4748−4756.

(8) Bonde, S.; Buch-Månson, N.; Rostgaard, K. R.; Andersen, T. K.; Berthing, T.; Martinez, K. L. Exploring Arrays of Vertical One-Dimensional Nanostructures for Cellular Investigations. *Nanotechnology* **2014**, *25*, 362001.

(9) Shalek, A. K.; Robinson, J. T.; Karp, E. S.; Lee, J. S.; Ahn, D. R.; Yoon, M. H.; Sutton, A.; Jorgolli, M.; Gertner, R. S.; Gujral, T. S.; MacBeath, G.; Yang, E. G.; Park, H. Vertical Silicon Nanowires as a Universal Platform for Delivering Biomolecules into Living Cells. *Proc. Natl. Acad. Sci. U. S. A.* **2010**, *107*, 1870−1875.

(10) Chiappini, C.; De Rosa, E.; Martinez, J. O.; Liu, X.; Steele, J.; Stevens, M. M.; Tasciotti, E. Biodegradable Silicon Nanoneedles Delivering Nucleic Acids Intracellularly Induce Localized in Vivo Neovascularization. *Nat. Mater.* **2015**, *14*, 532−539.

(11) Chiappini, C.; Martinez, J. O.; De Rosa, E.; Almeida, C. S.; Tasciotti, E.; Stevens, M. M. Biodegradable Nanoneedles for Localized Delivery of Nanoparticles in Vivo: Exploring the Biointerface. *ACS Nano* **2015**, *9*, 5500−5509.

(12) Chandrasekaran, S.; Macdonald, T. J.; Mange, Y. J.; Voelcker, N. H.; Nann, T. A. Quantum Dot Sensitized Catalytic Porous Silicon Photocathode. *J. Mater. Chem. A* **2014**, *2*, 9478−9481.

(13) Peng, K.-Q.; Wang, X.; Li, L.; Wu, X.-L.; Lee, S.-T. High-Performance Silicon Nanohole Solar Cells. *J. Am. Chem. Soc.* **2010**, *132*, 6872−6873.

(14) Gowda, S. R.; Pushparaj, V.; Herle, S.; Girishkumar, G.; Gordon, J. G.; Gullapalli, H.; Zhan, X.; Ajayan, P. M.; Reddy, A. L. M. Three-Dimensionally Engineered Porous Silicon Electrodes for Li Ion Batteries. *Nano Lett.* **2012**, *12*, 6060−6065.

(15) Jane, A.; Dronov, R.; Hodges, A.; Voelcker, N. H. Porous Silicon Biosensors on the Advance. *Trends Biotechnol.* **2009**, *27*, 230−239.

(16) Fu, J.; Wang, Y.-K.; Yang, M. T.; Desai, R. A.; Yu, X.; Liu, Z.; Chen, C. S. Mechanical Regulation of Cell Function with Geometrically Modulated Elastomeric Substrates. *Nat. Methods* **2010**, *7*, 733−736.

(17) Lowe, R. D.; Szili, E. J.; Kirkbride, P.; Thissen, H.; Siuzdak, G.; Voelcker, N. H. Combined Immunocapture and Laser Desorption/Ionization Mass Spectrometry on Porous Silicon. *Anal. Chem.* **2010**, *82*, 4201−4208.

(18) Lu, W.; Lieber, C. M. Semiconductor Nanowires. *J. Phys. D: Appl. Phys.* **2006**, *39*, R387−R406.

(19) Dick, K. A.; Deppert, K.; Martensson, T.; Mandl, B.; Samuelson, L.; Seifert, W. Failure of the Vapor-Liquid-Solid Mechanism in Au-Assisted MOVPE Growth of InAs Nanowires. *Nano Lett.* **2005**, *5*, 761−764.

(20) Pevzner, A.; Engel, Y.; Elnathan, R.; Ducobni, T.; Ben-Ishai, M.; Reddy, K.; Shpaisman, N.; Tsukernik, A.; Oksman, M.; Patolsky, F. Knocking Down Highly-Ordered Large-Scale Nanowire Arrays. *Nano Lett.* **2010**, *10*, 1202−1208.

(21) Huang, Z.; Geyer, N.; Werner, P.; de Boor, J.; Gosele, U. Metal-Assisted Chemical Etching of Silicon: a Review. *Adv. Mater.* **2011**, *23*, 285−308.

(22) Morales, A. M.; Lieber, C. M. A Laser Ablation Method for the Synthesis of Crystalline Semiconductor Nanowires. *Science* **1998**, *279*, 208−211.

(23) Hanarp, P.; Sutherland, D. S.; Gold, J.; Kasemo, B. Control of Nanoparticle Film Structure for Colloidal Lithography. *Colloids Surf., A* **2003**, *214*, 23−36.

(24) Hulteen, J. C.; Van Duyne, R. P. Nanosphere lithography: A Materials General Fabrication Process for Periodic Particle Array Surfaces. *J. Vac. Sci. Technol., A* **1995**, *13*, 1553−1558.

(25) Denkov, N.; Velev, O.; Kralchevski, P.; Ivanov, I.; Yoshimura, H.; Nagayama, K. Mechanism of Formation of Two-Dimensional Crystals from Latex Particles on Substrates. *Langmuir* **1992**, *8*, 3183−3190.

(26) Dimitrov, A. S.; Nagayama, K. Continuous Convective Assembling of Fine Particles into Two-Dimensional Arrays on Solid Surfaces. *Langmuir* **1996**, *12*, 1303−1311.

(27) Kraus, T.; Brodoceanu, D.; Pazos-Perez, N.; Fery, A. Colloidal Surface Assemblies: Nanotechnology Meets Bioinspiration. *Adv. Funct. Mater.* **2013**, *23*, 4529−4541.

(28) Lumsdon, S. O.; Kaler, E. W.; Williams, J. P.; Velev, O. D. Dielectrophoretic Assembly of Oriented and Switchable Two-Dimensional Photonic Crystals. *Appl. Phys. Lett.* **2003**, *82*, 949−951.

DOI: 10.1021/acsami.5b07777
ACS Appl. Mater. Interfaces 2015, 7, 23717−23724

(29) Zhang, K. Q.; Liu, X. Y. In Situ Observation of Colloidal Monolayer Nucleation Driven by an Alternating Electric Field. *Nature* **2004**, *429*, 739−743.
(30) Blattler, T. M.; Binkert, A.; Zimmermann, M.; Textor, M.; Voros, J.; Reimhult, E. From Particle Self-Assembly to Functionalized Sub-Micron Protein Patterns. *Nanotechnology* **2008**, *19*, 075301.
(31) Plettl, A.; Enderle, F.; Saitner, M.; Manzke, A.; Pfahler, C.; Wiedemann, S.; Ziemann, P. Non-Close-Packed Crystals from Self-Assembled Polystyrene Spheres by Isotropic Plasma Etching: Adding Flexibility to Colloid Lithography. *Adv. Funct. Mater.* **2009**, *19*, 3279−3284.
(32) Isa, L.; Kumar, K.; Müller, M.; Grolig, J.; Textor, M.; Reimhult, E. Particle Lithography from Colloidal Self-Assembly at Liquid-Liquid Interfaces. *ACS Nano* **2010**, *4*, 5665−5670.
(33) Pieranski, P. Two-Dimensional Interfacial Colloidal Crystals. *Phys. Rev. Lett.* **1980**, *45*, 569.
(34) Binks, B. P.; Lumsdon, S. O. Influence of Particle Wettability on the Type and Stability of Surfactant-Free Emulsions. *Langmuir* **2000**, *16*, 8622−8631.
(35) Ray, M. A.; Jia, L. Micropatterning by Non-Densely Packed Interfacial Colloidal Crystals. *Adv. Mater.* **2007**, *19*, 2020−2022.
(36) Scheeler, S. P.; Ullrich, S.; Kudera, S.; Pacholski, C. Fabrication of Porous Silicon by Metal-Assisted Etching Using Highly Ordered Gold Nanoparticle Arrays. *Nanoscale Res. Lett.* **2012**, *7*, 450−450.
(37) Pla-Roca, M.; Isa, L.; Kumar, K.; Reimhult, E. Selective (Bio)Functionalization of Solid-State Nanopores. *ACS Appl. Mater. Interfaces* **2015**, *7*, 6030−6035.
(38) Kim, J.; Kim, H. N.; Lim, K. T.; Kim, Y.; Seonwoo, H.; Park, S. H.; Lim, H. J.; Kim, D. H.; Suh, K. Y.; Choung, P. H.; Choung, Y. H.; Chung, J. H. Designing Nanotopographical Density of Extracellular Matrix for Controlled Morphology and Function of Human Mesenchymal Stem Cells. *Sci. Rep.* **2013**, *3*, 3552.
(39) Rizk, A.; Rabie, B. M. Electroporation for Transfection and Differentiation of Dental Pulp Stem Cells. *BioRes. Open Access* **2013**, *2*, 155−162.

DOI: 10.1021/acsami.5b07777
ACS Appl. Mater. Interfaces 2015, 7, 23717−23724